Investigation of the structural control of a deltaic valley with geophysical methods. The case study of Pineios river delta (Thessaly, Greece).

Spyridon Dilalos[1], John D. Alexopoulos[1], Emmanuel Vassilakis[2], Serafim E. Poulos[2]

[1] National and Kapodistrian University of Athens, Department of Geology and Geoenvironment, Division of Geophysics-Geothermy, Panepistiomioupoli Zografou, Greece

[2] National and Kapodistrian University of Athens, Department of Geology and Geoenvironment, Division of Geography-Climatology, Panepistiomioupoli Zografou, Greece

Abstract

The current study aims to clarify the structural regime of the deltaic valley of Pineios river (Thessaly, Greece). The structural control of a deltaic area is usually a crucial parameter for its Palaio-geographical evolution and the latter needs to be clear for the contemporary conservation of such a sensitive ecotope environmentally. The investigation of the concealed subsurface tectonic structures was accomplished through the combined interpretation of gravity measurements, VES and TEM soundings. The standard gravity data reduction has been carried out and the residual anomaly was isolated with the contribution of the Fourier filters. The Euler deconvolution has been applied, providing the corresponding depth solutions between 159.8 and 1,716.6 meters. In the context of the qualitative interpretation, we produced several structural maps (THDR, VDR, Tilt and Theta) in order to enhance the edges of density sources that may reflect fault zones. Severe indications for the delineation of fault zones of the area were provided by these maps. Moreover, 3D density models of the area have been constructed illustrating the subsurface density distribution, up to depths of 3,370 meters. A main zone of lower densities in the central part of the delta has been revealed, surrounded by three zones of higher densities. Afterwards, the densities of the majority of the existing geological formations were determined with laboratory measurements from geological specimens. Therefore, three geophysical-geological profiles have been constructed, based not only on the gravity modelling but also on the geological interpretation of the geoelectrical layered models from the VES and TEM measurements. In conclusion, concealed and unknown tectonic structures of the Pineios deltaic valley have been identified beneath the surface.

Keywords: Gravity method, Vertical Electrical Sounding, Transient Electromagnetic method, structural maps, 3D model

1. Introduction

Deltaic systems are relatively complex geological environments, subject to a range of fluvial, climatic, tectonic, sea level controls and anthropogenic activity; the latter is mostly related to the control of freshwater and sediment fluxes (e.g. dam construction) (Vörösmarty *et al.*, 2003) and also subsidence (Syvitski, 2008). In the highly tectonically active eastern Mediterranean region, the knowledge of the geological structure is vital for the reconstruction of the palaeo-relief on top of which the modern delta has been formed, defining also flow paths of the river and its possible changes (Gaki-Papanastassiou et al., 2011). Thus, the knowledge of the geological structure and the relief of the alpine basement is a crucial parameter for the overall formation of the deltaic system.

The determination of the structural regime of the deltaic valley of Pineios river is a crucial parameter for comprehending its Palaio-geographical evolution. Beyond the surface geological mapping revealed by previous studies, it is very important to gather more information regarding the subsurface deltaic structure. For that reason, the present study aims to investigate the deeper geological alpine structure of the deltaic plain of Pineios river, through the combined application of gravity measurements, Vertical Electrical Soundings (VES) and Transient Electromagnetic Soundings (TEM). The delta of Pineios River, which is the third longest river in Greece, drains the eastern part of central Greece debouch to the western coast of the outer Thermaikos Gulf; the latter is a geologically active area, regarding the post-alpine tectonic regime. Moreover, the present investigation may contribute to the recognition of the exact time period of the opening of Tempi valley that it is placed after the Villafranchian (3.2-1 Ma) (Migiros *et al*., 2011).

On the basis of the results of some preliminary geophysical research in the area, the results of applying the Vertical Electrical Soundings (VES) and Transient Electromagnetic Soundings (TEM) in the deltaic area of Pineios have somehow been discussed in the past by the authors (Alexopoulos, 2014; Alexopoulos *et al*., 2014a; 2014b; 2019; Matiatos *et al*., 2018), but mainly focused on hydro-geophysical characterization and the adumbration of the deltaic aquifers. The present study aims to investigate the deeper geological structure of the deltaic valley of Pineios river, through the combined application of gravity measurements, Vertical Electrical Soundings (VES) and Transient Electromagnetic Soundings (TEM).

The authors have not found in the literature such a combination of geophysical methods for the investigation of the deltaic deeper subsurface. On the other hand, some of these geophysical methods have been adopted in other deltaic environments of the world. For example, focused on hydro-geophysical investigations, a geoelectrical investigation of the Wadi El-Arish delta in Egypt has been conducted (Khalil & Santos, 2011), the geoelectrical mapping of Camargue Deltaic plain in France (Torres-Rondon *et al*., 2013) and the application of VES and TEM at west Nile delta regions (Ibraheem et al., 2016; Othman *et al*., 2019). Other cases of deltaic geophysical research, by mainly based on gravity or/and seismic methods and focused on structural purposes have been presented, such as the case of Mahanadi delta of eastern India

(Behera *et al*., 2004), the Colorado delta region (Kovach *et al*., 1962), the Niger Delta in West Africa (Hospers, 2015) and the west Nile region in Egypt (Saleh, 2013).

2. Geological Setting

The deltaic plain covers an area of 69 km^2 consisting of fluvial-shallow marine deposits, boarded towards the sea by sandy gravelly deposits in the form of beach barriers and successive beach ridges (Lazogiannis *et al*., 2015; Karymbalis *et al* 2016). The remnants of a Pleistocene alluvial fan are observed in the western part of the delta plain and lie uncomfortably on Neogene formations comprised of sandstones, conglomerates and terra rossa (Katsikatsos & Migkiros, 1982). The Pineios delta, is relatively small relatively to its large catchment (10.000 km^2); this is related to overall geological structure (e.g. water depths in excess of 300 m) and to the opening of Tempi valley. The latter is a deep gorge, formed by the river erosion in karstified limestones and located in between the mountains of Olympus (north) and Ossa (south), connecting the main alluvial plain of Thessaly with the deltaic plain, acting also as a temporary base level for the whole drainage basin of Pineios river.

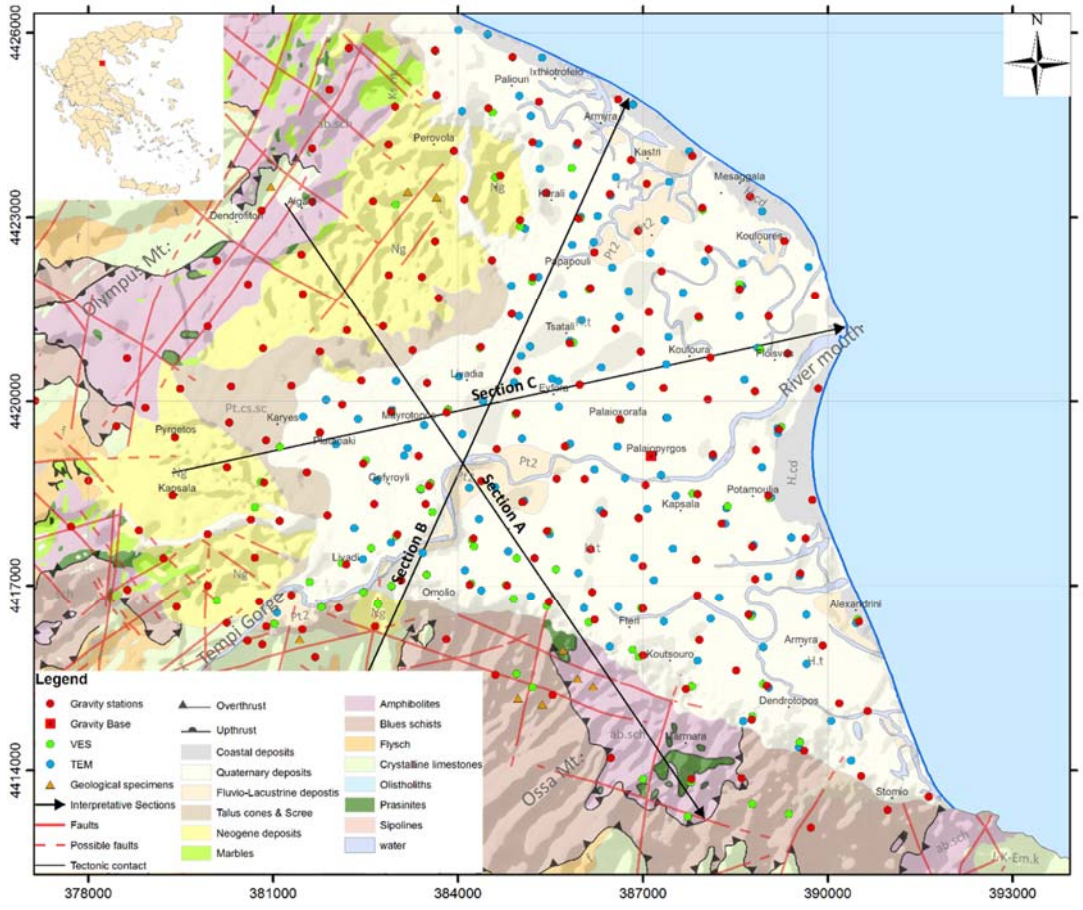

Figure 1: Geological and tectonic map (modified by Katsikatsos & Migkiros, 1982) along with the locations of all the geophysical measurements and interpretative models (§4.2). Finally, the field samples for the laboratory measurements are illustrated (§4.1). The red rectangle on the index map indicates the location of the study area.

The Neogene formations, with alternations of sands, marls and conglomerates occupy almost the entire space of the subsurface deltaic field, below the Holocene deposits.

At the southern and northern margins of the deltaic area (Fig. 1), the alpine basement is cropping out including various lithologies, such as metamorphic flysch and crystalline limestones (Ossa-Olympos unit), blue schists, marbles and gneisses (Ambelakia unit), marbles and metamorphic basic ophiolitic rocks (Pelagonian unit). Based on Vassilakis *et al*. (2014), the Neogene formations have undergone intense tectonic deformation resulting in the tilting of several blocks, reaching the values of 10-30^{o}, towards south. The horizontally deposited Neogene formations became inclined, due to the activity of an NNW dipping normal fault zone, which is located south of *Omolio* village, striking WSW-ENE. The activity of this fault zone is highly connected to the formation of Tempi gorge, which connects the main hydrologic basin of Pineios with its delta. A clearly formed fault scarp that is found on crystalline limestones, was measured during the fieldwork. The fault plane is dipping 65^{o}, whilst its dip direction was measured at 310^{o}. It hosts kinematic indicators (striations, slickensides) that are in agreement with extensional deformation through normal displacement.

The SSE striking northern foothills of Ossa Mt, consisting of alpine basement rocks, bound the deltaic basin, implying that there is a highly active fault zone but without any surface structural expressions (relief discontinuities, fault planes etc.). Moreover, Ossa's Mt alpine basement formations (at the southern part of the delta), have been identified only by the geophysical soundings near the margins, with a gentle inclination below the post-alpine sediments, for the depths of investigation up to 200-250 meters (Vassilakis *et al*., 2014).

3. Methodology

An extensive geophysical survey has been conducted along the deltaic area of Pineios River for the delineation of the subsurface structure. In this paper, we will interpret the results of the integrated geophysical survey that has been conducted in the area.

3.1 Gravity method

In the past gravity surveys have been conducted for the delineation of the tectonic structure of deltaic areas (Behera *et al*., 2004; Fairhead & Okereke, 1987; Hospers, 1965; ElGalladi *et al*., 2009; Kovach *et al*., 1962; Saleh, 2013; Selim, 2013).

A gravity survey has been carried along the deltaic area and the foothills of the surrounding mountains. The gravity measurements were planned on a grid, with an initially station grid spacing equal to 1km. After the processing of the first measurements, some denser stations had been added in between, in order to clarify the status of some ambiguous areas. The gravity database is comprised of 177 gravity stations (Fig. 1) and one gravity base that has been established at the "*Palaiopyrgos*" village (*Easting: 387130.104, Northing: 4419106.704, Elevation: 4.361 in EGSA'87 meters*). The gravity base (*Absolute value: 980166.62 mGal*) is referred to the IGSN'71 datum (Morelli *et al*., 1974) as it was tied to a previously established

gravity base (Dilalos, 2018; Dilalos & Alexopoulos, 2019a; Dilalos & Alexopoulos, 2020). All the measurements were carried out during the summer of 2015 with a LaCoste & Romberg G-496 gravity meter. The necessary coordinates of each gravity station have been measured with differential Global Navigation Satellite System (dGNSS), compiled by two different, dual-frequency TopCon HiperPro GPS antennas and the establishment of a local topographic base at '*Mesaggala*" village. The coordinates were calculated in the Hellenic Geodetic Reference System 1987.

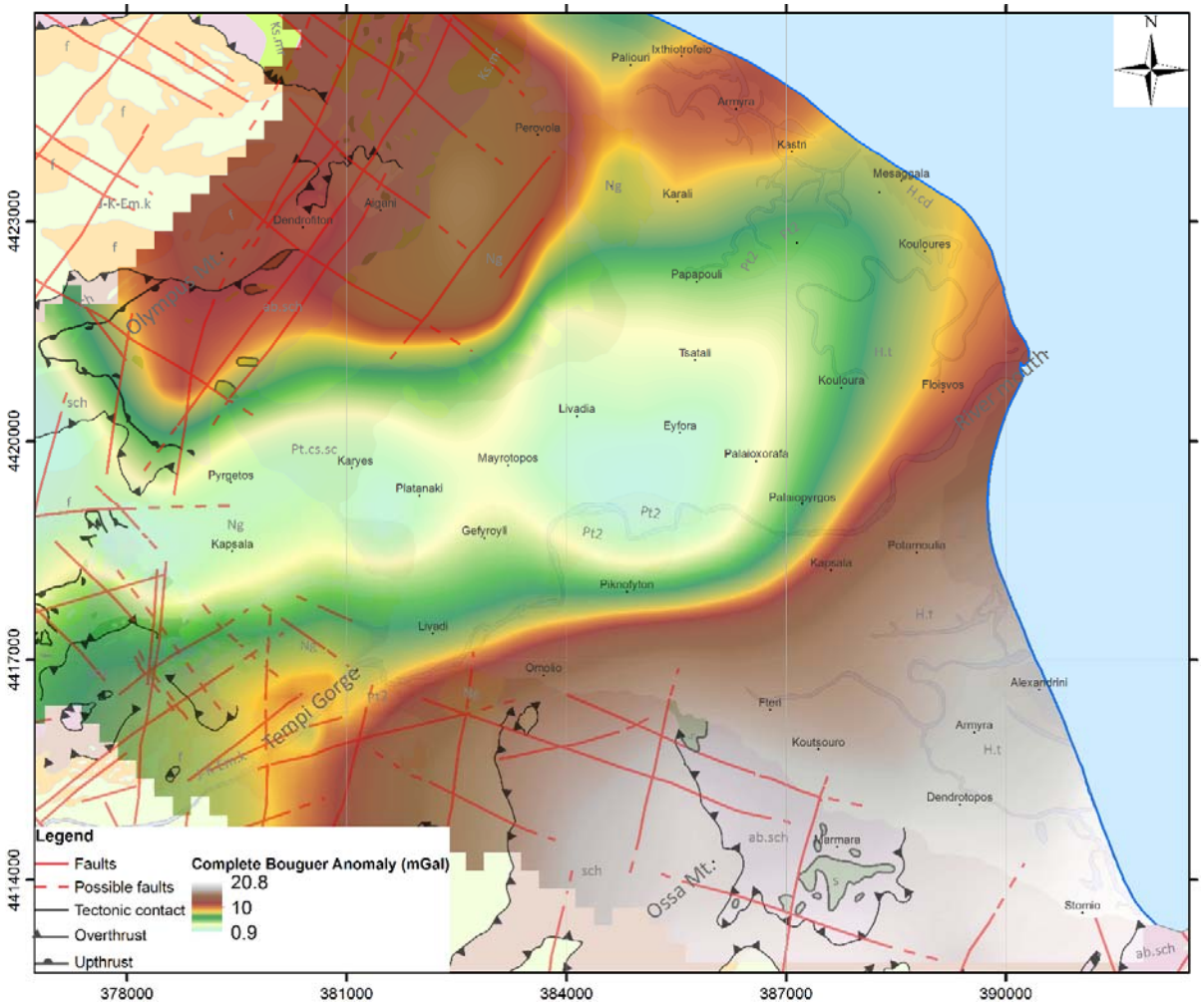

Figure 2. Complete Bouguer anomaly map of Pineios deltaic valley.

The data reduction procedure (drift, tide, latitude and free-air corrections) was carried out with the Oasis Montaj software. The assumed constant density for the Bouguer correction was set up to 2.67gr/cm^3, generally used by several other researchers (Dilalos & Alexopoulos, 2017; 2019b; Dilalos *et al*., 2018). Therefore, the Simple Bouguer Anomaly has been calculated. In order to calculate the necessary terrain correction, we took advantage of a Digital Elevation Model (DEM) and the Gravity and Terrain Correction extension of Oasis Montaj, with an inner radius equal to 1.500 meters and an outer one equal to 21 kilometers. The Complete Bouguer Anomaly Map calculated after the application of the terrain correction is illustrated in Figure 2, with values

ranging between 0.9 and 20.8 mGal. The higher values are located mostly at the mountainous area in the northern and southern area.

The regional-residual separation was accomplished with the application of the Gaussian filter through the MAGMAP extension of Oasis Montaj software (Anudu *et al*., 2016; Damaceno *et al*., 2017; Dilalos & Alexopoulos, 2021; Dilalos *et al*., 2019a). The corresponding Power Spectrum Analysis of the Complete Bouguer data (Fig. 3) was taken into consideration for the separation of the regional and residual gravity fields. Based on its results, two different depths of the anomaly sources seem to have been identified, at 1.51 km and 0.55 km depth.

Consequently, we produced a residual map with a cutoff wavelength of 500m and standard deviation equal to 0.4 cycles/km mainly for the relatively shallow structures and a second residual map of the basement, with standard deviation equal to 0.06 cycles/km, including the anomaly sources and information from deeper structures of the bedrock. The values of the residual map of the basement (Fig. 4) range from -4.59 mGal to 4.97 mGal, with the contribution of both deep and shallow structures. The values of the residual map of the shallow anomaly sources and structures (Fig. 5) range from -0.97 mGal to 1.04 mGal.

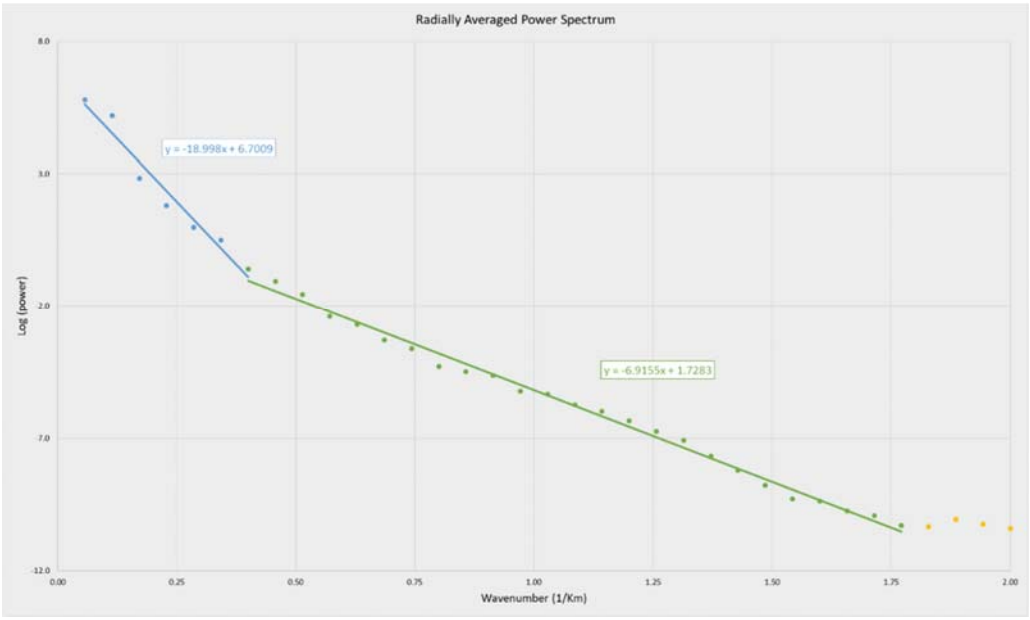

Figure 3. Radially Averaged Power Spectrum

3.1.1 Euler deconvolution

The outcome of the Euler deconvolution here is a map, illustrating the locations and depths of the geologic sources of gravity anomalies that have been identified in grid-based gravity data, like in several other cases (Dilalos & Alexopoulos, 2019b; 2020; Khalil *et al.,* 2014; Martins-Ferreira *et al*., 2018; Selim, 2013).

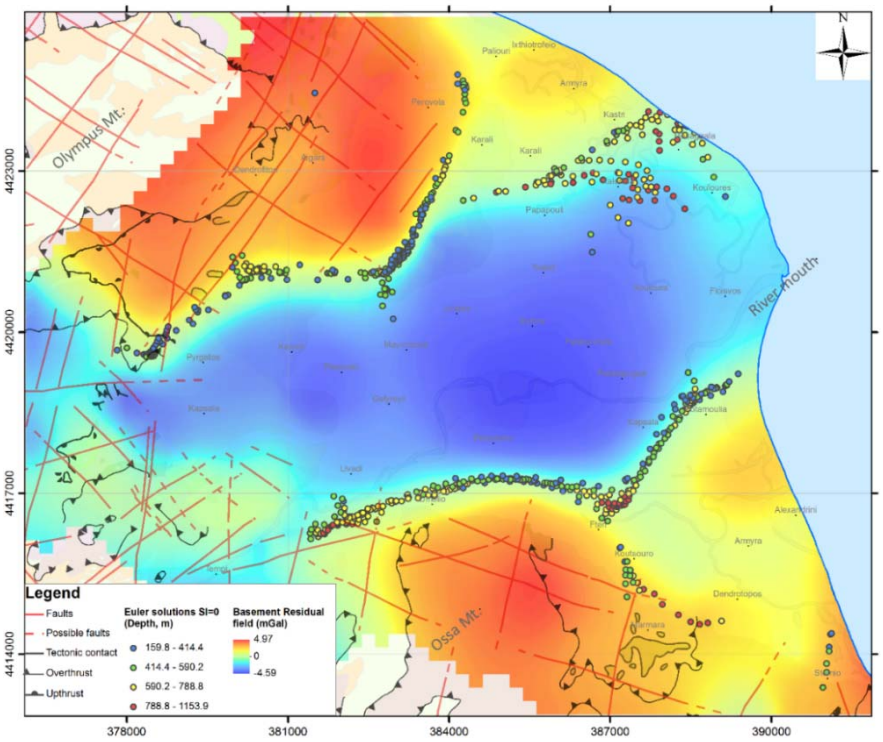

Figure 4. Residual maps of deeper structures (0.06 cycles/km), along with the Euler solutions (graduated symbols with depth) for SI=0

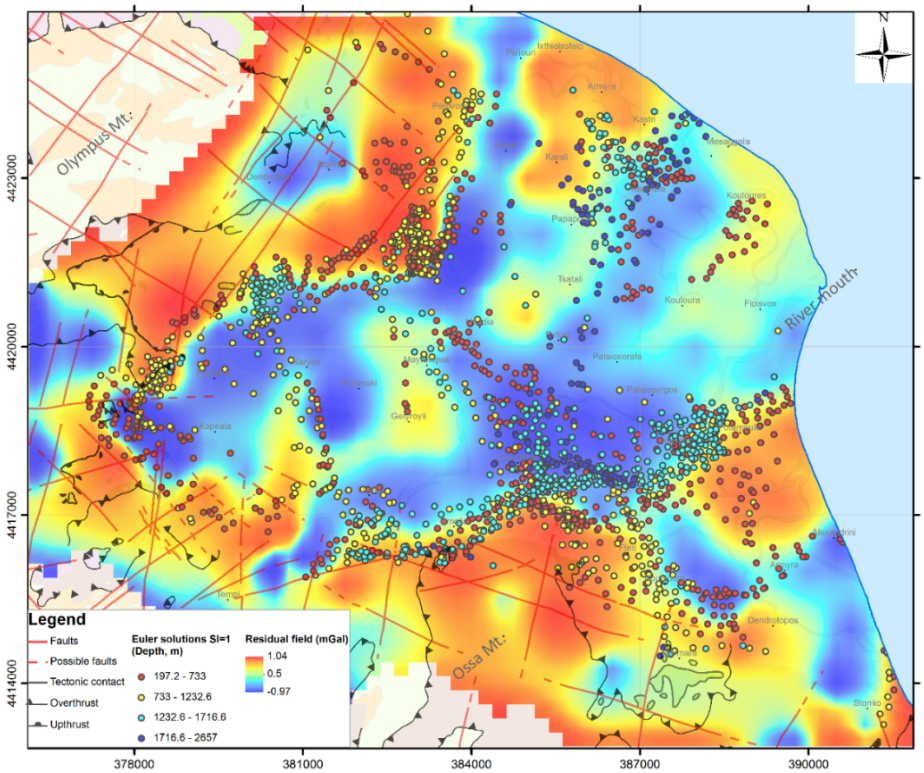

Figure 5. Residual maps of relatively shallow structures (0.4 cycles/km) along with the Euler solutions (graduated symbols with depth) for SI=1

In the context of this paper, we have calculated Euler depth solutions with the *Euler3D* extension of *Oasis Montaj* software, by using Structural Index (SI) values equal to 0 (Fig. 4) and 1 (Fig. 5), since both are considered to be close to the fault/contact type that we want to delineate. The window size was set to 15x15 grid points.

The produced solutions for Structural Index zero (0) are mainly located along two linear clusters, in the northern and southern area, with a main direction of NW-SE and secondary NNW-SSE. Both of them are located close to the foothills of the two surrounding mountains. The southernmost one, at a point, turns away from the foothills of Ossa Mt, indicating a 'path' of solutions towards the inner deltaic basin. They are observed in the basement residual map (Fig.4), with depths mostly between 159.8 and 788.8 meters and some deeper (788.8-1,154 m) at the western area.

For the Structural Index equal to one (1), the produced Euler solutions are more. We can also observe similar linear clusters of solutions with the Structural Index zero, but we can also observe some more clusters crossing the deltaic area. The direction of these clusters is almost perpendicular to the previous ones, that is NNE-SSW. They are observed in the residual map (Fig.5), with greater depths, mostly between 197.2 and 1,716.6 meters, but also some deeper (1,716.6-2,657 m) at the southern area of the basin.

As we can see, the two different depths of the anomaly sources that have been identified from the Energy Spectrum (at depths of 550 meters and 1,510 meters), are in good accordance with the Euler solutions that have been calculated above. More specifically, the Euler solutions for Structural Index 0 (depths mostly between 159.8 and 788.8 meters) seem to correspond to the shallower anomaly sources located at the depth of 550 meters. On the other hand, the Euler solutions for Structural Index 1 (depths mostly between 197.2 and 1,716.6 meters) seem to include both the shallow and deeper anomaly sources (550 and 1,510 meters correspondingly).

3.1.2. Structural mapping

At this point we will produce some structural maps of the deltaic area in order to enhance the existent structural edges. It is a helpful and successful approach in structural investigations (Ali *et al*., 2017; Anudu *et al*., 2016; Dilalos *et al*., 2019a; Khalil *et al*., 2014; Martins-Ferreira *et al.,* 2018; Nasuti *et al*., 2012; Selim, 2013).

The THDR and VDR maps are considered to be related and controlled by the lateral variation in density of the source bodies and therefore with the geology (Fairhead, 2015). On the other hand, the so-called local phase derivatives (Tilt and Theta maps), are considered to be more independent of density.

Firstly, the results of the **Total Horizontal Derivative (THDR)** are illustrated in Figure 6 for the shallow sources and in Figure 7 for the deeper ones. In these maps, the maximum values tend to identify linear edges (e.g. fault zones or contacts), especially for shallow structures. The **THDR** results for the deeper structures (Fig. 7) reveal an image similar to the one of Euler solutions with

Structural Index 0 (Fig. 4) and two main zones of NW-SE direction along. There are also two relatively perpendicular zones to them (direction N-S), one at the northern area and one at the central part of the valley. The **THDR** map of the shallower structures (Fig. 6) is more complicated, revealing more traces of possible edges at the interior of the delta, with two dominating directions, WWS-EEN and NNW-SSE.

The results of the **First Vertical Derivative (VDR)** are illustrated in Figure 8 (shallow structures) and Figure 9 (basement structures). This technique is also more sensitive to the shallow structures (Fairhead, 2015). In the **VDR** and **Tilt derivative** maps (Figs. 8-11), the zero crossing adumbrate the edge location while the maxima values outline the structure location providing at the same time information about its positive or negative density and therefore for its dip. Practically in all these maps (Figs. 8-11) we have masked the areas with the negative values of the derivative (Ali *et al.,* 2017; Dilalos *et.,* 2019; Nasuti *et al*., 2012) aiming to simplify them. Therefore, only the structural edges (zero crossings) and the positive structures-possible horsts only (maxima) are illustrated. The results of the **VDR** (Figs. 8-9) indicate almost the same edges as those of the **THDR** (Figs. 6-7) but also providing information about the relative block position (positive density bodies). Beyond that, the **VDR** and **Tilt derivative** maps (Figs. 10-11) provide almost identical images, for both shallow and deeper structures.

Finally, for the **Theta derivative** maps (Wijns *et al.*, 2005) (Figs. 12-13) the edges are expected to be revealed by the maximum values equal to 1, or at least >0.80 (the units are in radians), based on the fact that it is practically the cosine of Tilt derivative. In the produced Theta maps (Figs. 12-13) we have also isolated the values greater than 0.8, trying to produce more perspicuous images. We could say that the image of the adumbrated edges is close to that of the previously mentioned structural maps.

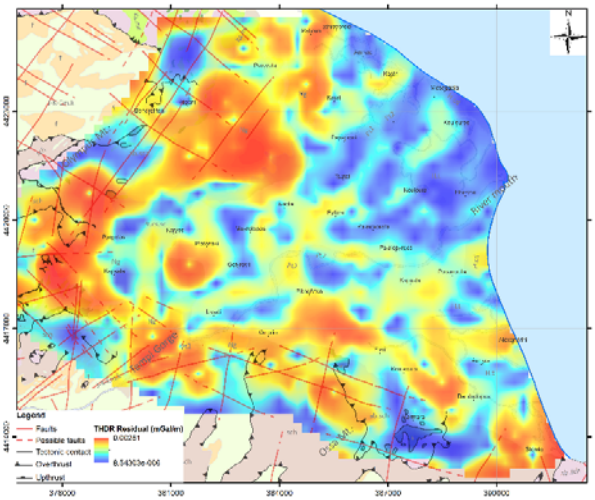

Figure 6. THDR of residual data (shallow structures).

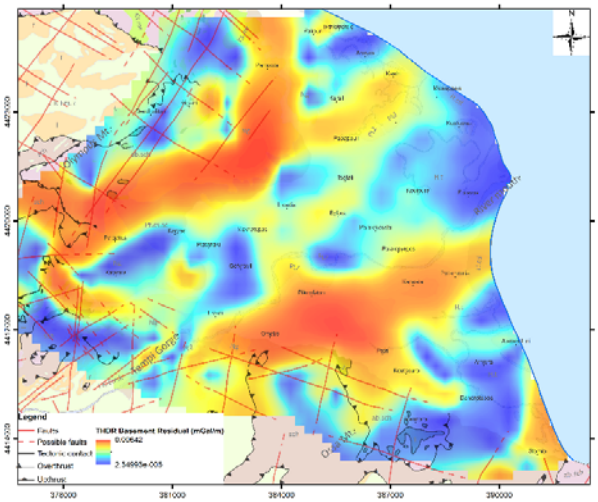

Figure 7. THDR of basement residual data (deep structures).

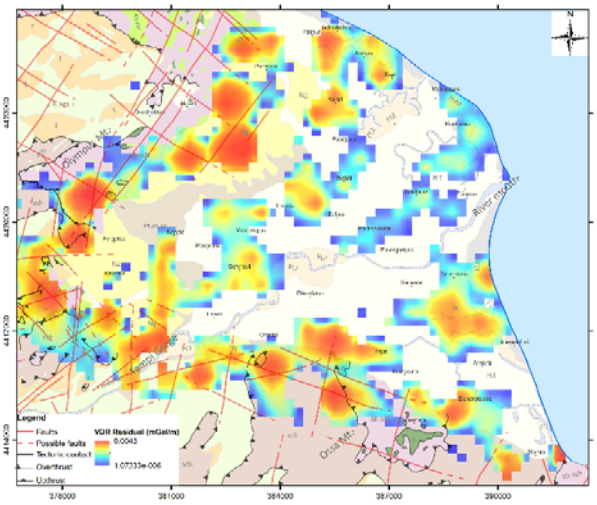

Figure 8. VDR of residual data (shallow structures).

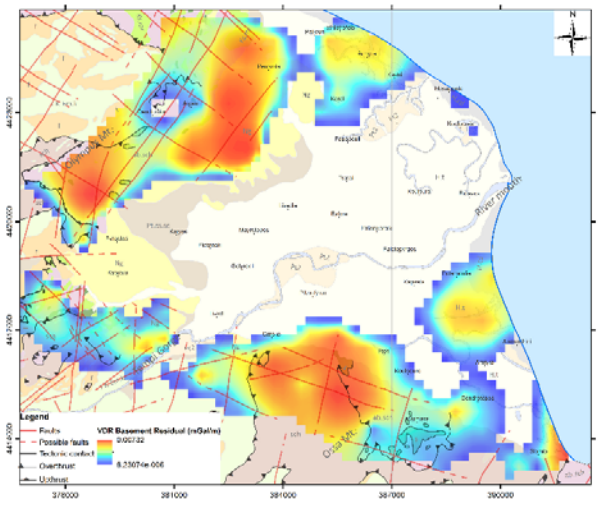

Figure 9. VDR of basement residual data (deep structures).

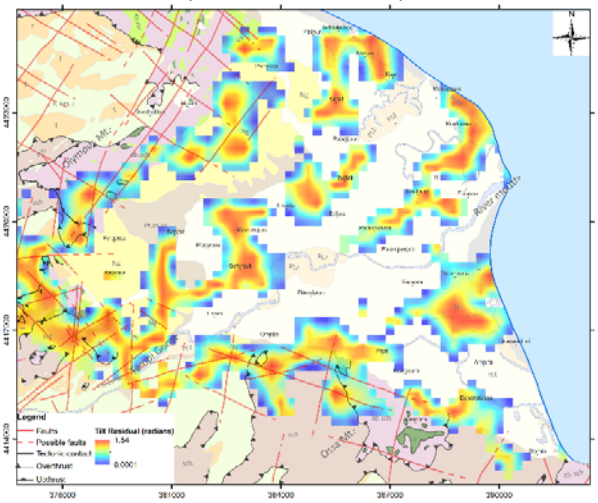

Figure 10. Tilt derivative of residual data (shallow structures).

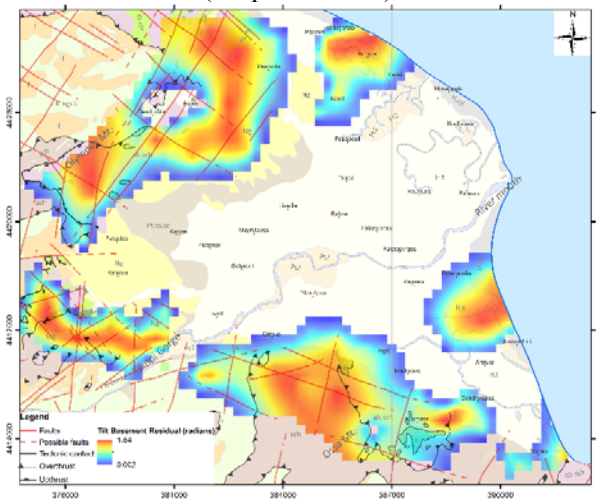

Figure 11. Tilt derivative of basement residual data (deep structures).

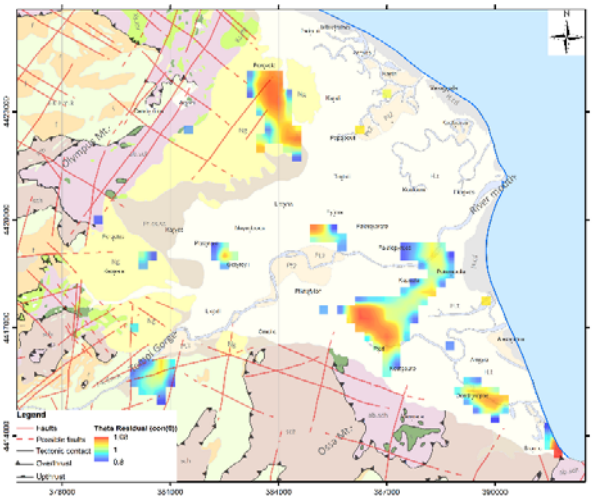

Figure 12. Theta derivative of residual data (shallow structures).

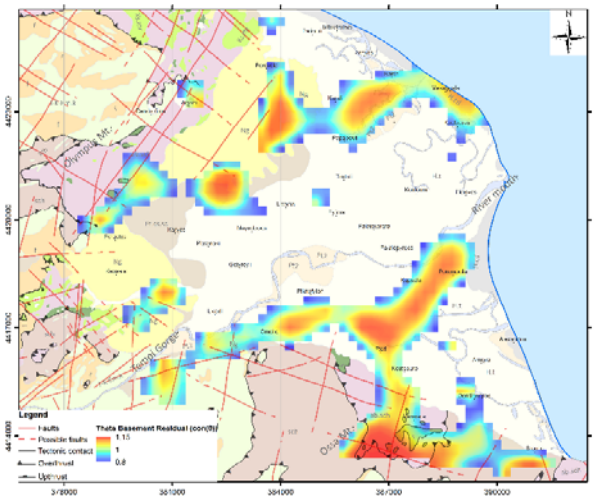

Figure 13. Theta derivative of basement residual data (deep structures).

3.1.3 3D density models

A 3D gravity model will provide a density distribution of the subsurface structure of the basin , based on a mesh of blocks with individual density values (Andersson & Malehmir, 2018; Azizi & Saibi, 2015; Bersi *et al.,* 2016; Boszczuk *et al.,* 2011; Damaceno *et al.,* 2017; Dilalos & Alexopoulos, 2019b; 2020).

In the context of this paper we used the "*VOXI*" Earth modelling module (Azizi & Saibi, 2015; Dilalos & Alexopoulos, 2020; Martins-Ferreira *et al*., 2018; Weidmann *et al.,* 2016) of Oasis Montaj by Geosoft for the density inversions. We applied the unconstrained 3D gravity modelling on the Residual anomaly data. The subsurface was first discretized in a 3D block mesh, where all blocks have a cell size equal to 500 meters. Practically, the produced block mesh is constituted by a total of 12,096 blocks of individual density contrast. The density contrast ranges from -0.131 gr/cm^3 (bluish colors) to 0.122 gr/cm^3 (reddish colors), with a maximum depth of almost 3,370 meters (absolute elevation -3,620m). Beyond that, in Figure 14 we provide an alternative pseudo-3D view based on the depth slices (Andersson & Malehmir, 2018; Bersi *et al.,* 2016; Dilalos & Alexopoulos, 2020) of the inversion model we have calculated for a better understanding of the subsurface density structure.

In Figure 15, we have isolated the bodies with negative density contrast (ranging from -0.131 to -0.02 gr/cm^3) producing the low gravity anomalies in the Residual maps (Figs. 4-5). On the other hand, in Figure 16, the bodies with positive density contrast are illustrated (0.02-0.122 gr/cm^3), producing the high gravity anomalies.

The results of the 3D models (Figs. 14-16) are quite impressive and revealed important subsurface structures of the deltaic area that might play important role for the structural control and Palaio-geographical evolution of the delta. Practically, a main zone of lower densities in the central part of the delta has been revealed, surrounded by three zones of higher densities. Between these zones, we could expect the existence of fault zones or tectonic contacts (e.g. upthrusts and overthrusts).

These 3D density models provide quantitative data for the subsurface that have been taken into consideration for the geological modelling (Fig. 20), since we can observe both vertical and lateral changes of the density and therefore, we can have a first correlation with the geological subsurface structure. By observing this zone of low densities in Figure 15 (along with the results of Figure 16) we firstly realized that the Crystalline limestones (J-K-Em.k) may practically form this zone, taken into account that their density is lower than the one of the overlying Blue Schists (*sch*). This zone was the guidance for the interpretation of the geophysical-geological profiles that are illustrated in Figure 20, where we observe the Crystalline limestones in the middle part of sections.

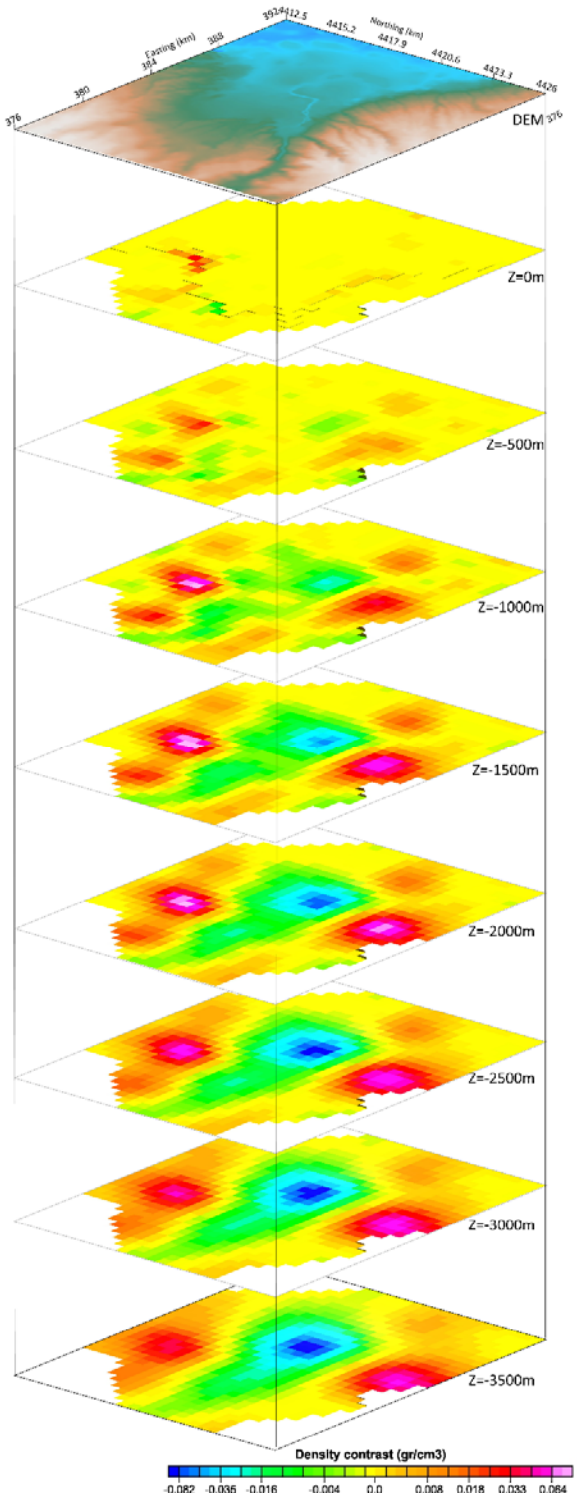

Figure 14. Depth slices of the 3D gravity inversion model of deltaic area. The upper plane illustrates the DEM of the area. The view angle is from the gorge of Tempi towards the river mouth.

252

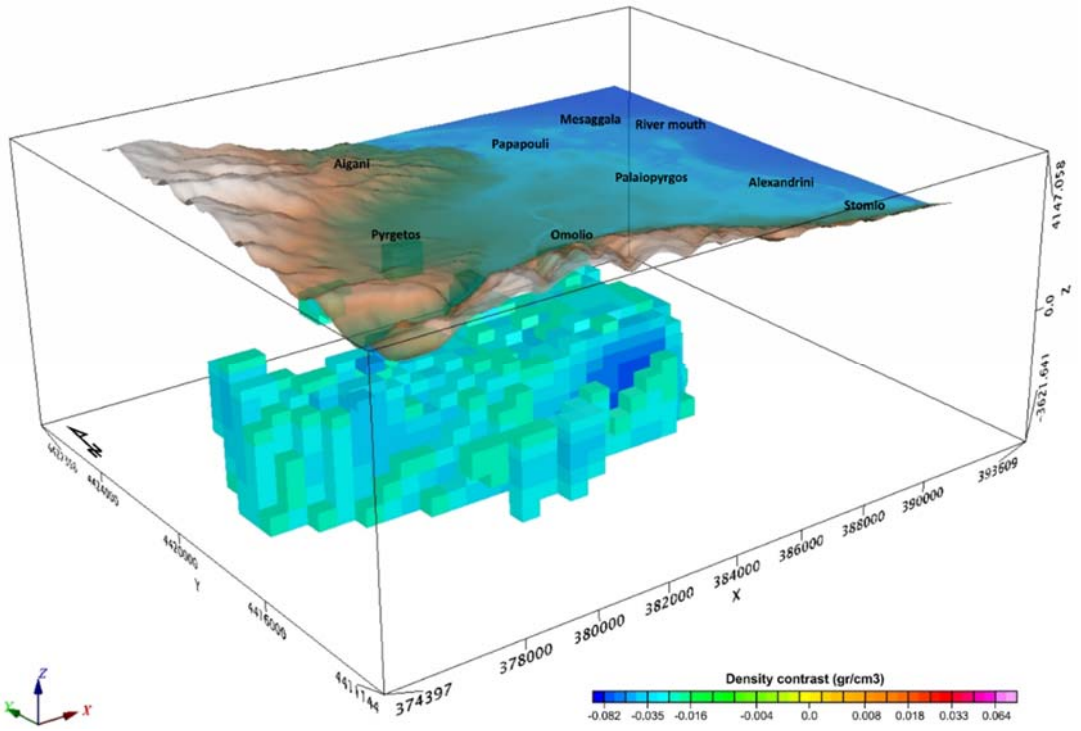

Figure 15. 3D gravity inversion (cell size 500m, mesh 32x27x14 blocks), showing structures of low densities (density contrast from -0.131 to -0.02 gr/cm^3).

253

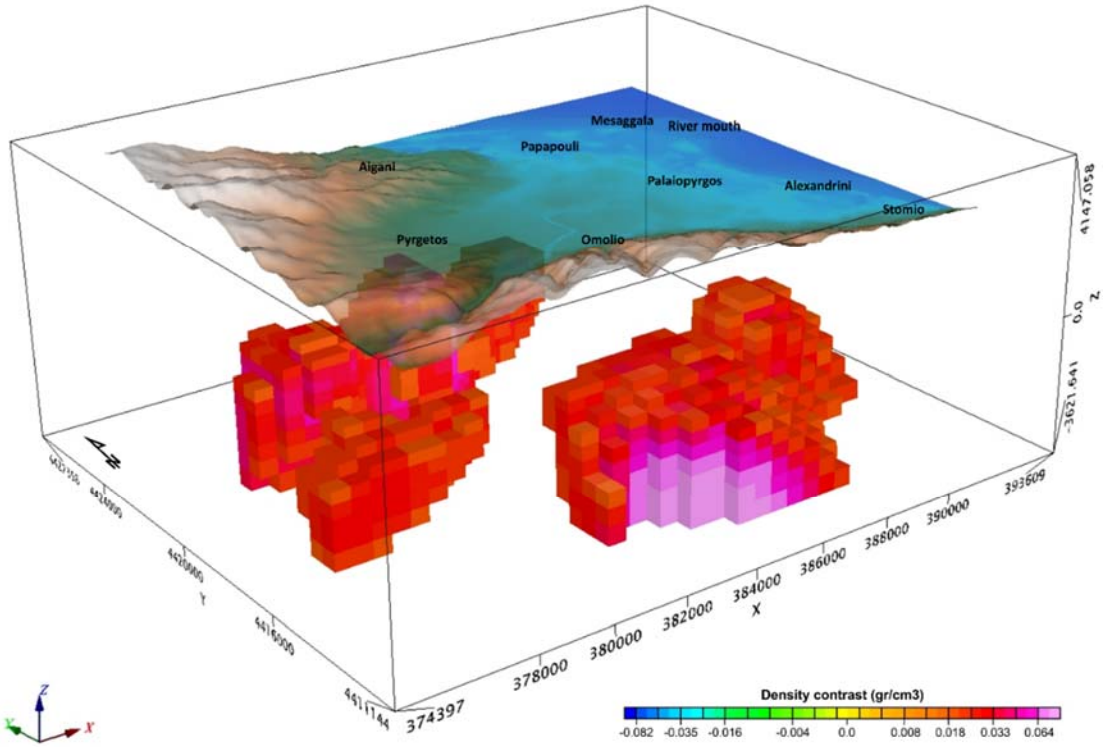

Figure 16. 3D gravity inversion (cell size 500m, mesh 32x27x14 blocks), showing structures of high densities (density contrasts from 0.02 to 0.122 gr/cm^3).

3.2 Geoelectrical and Geoelectromagnetic methods

The geoelectrical method and more specifically the Vertical Electrical Soundings (VES) have been applied successfully by several authors (Ibraheem *et al*., 2016; Khalil & Santos, 2011; Othman *et al*., 2019) along deltaic areas for geological interpretation. Through the application of this method we can investigate relatively large depths and reveal geological information, based on the vertical distribution of their electrical resistivity. The Transient Electromagnetic Method (TEM) is a method that has been successfully combined with the Vertical Electrical Soundings for the determination of the subsurface geological structure (Alexopoulos *et al.,* 2017; 2019b; Barsukov & Fainberg, 2020; Othman *et al*., 2019;) and especially for deltaic areas (Ibraheem *et al*., 2016) .

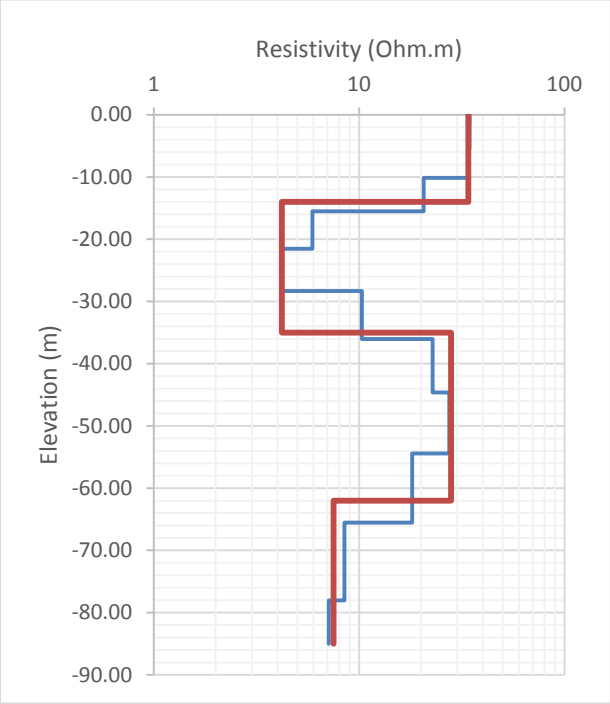

Figure 17. The geoelectrical model of the same TEM sounding is illustrated as a multi-layer model (*blue line*) and as a layered model (*red line*).

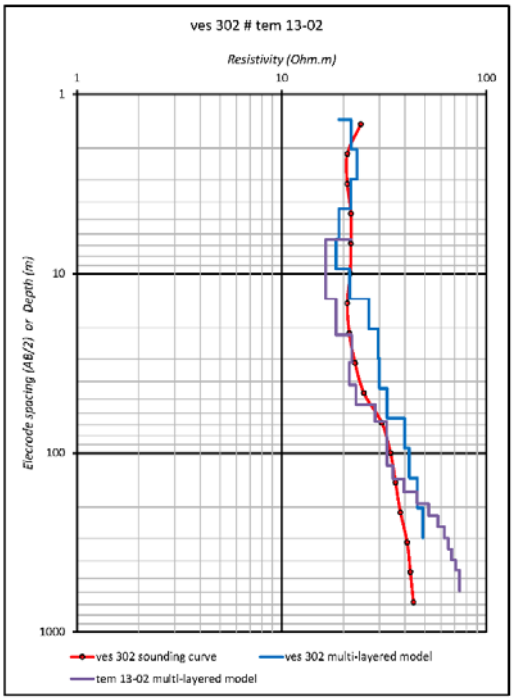

Figure 18. The red line illustrates the curve of VES 302. Its multi-layer model is illustrated with the blue line. The multi-layer model of TEM 13-02 (executed in the same area) is illustrated with the purple line.

In the context of the geophysical research in the region, a grid of forty-one (41) Vertical Electrical Soundings (VES) with Schlumberger array was carried out during the summer months (Fig. 1), investigating the resistivity distribution (Alexopoulos, 2014; Alexopoulos *et al*., 2014a; 2014b). The maximum current electrode spacing (AB) was 1400 m, achieving an investigation depth of almost 200-250 meters. The field measurements were carried out with an ABEM Terrameter System. The geoelectrical data, initially presented as field curves, were matched with the standard master and auxiliary curves for known layer parameters by Orellana and Mooney

(1966). Afterwards, they were processed by applying the automatic method of Zohdy (1989), composing a "multilayer" model. Finally, the Interpex commercial software package IX1D was used to produce the "layered" model. The initial geoelectrical model for the IX1D inversion procedure was the one that was calculated from the master curves Orellana and Mooney (1966). Moreover, another twenty-one (21) VES from the literature (Atzemoglou, 2010), located at the northern part of the delta, were re-processed and re-evaluated by the authors using the prementioned processing procedure.

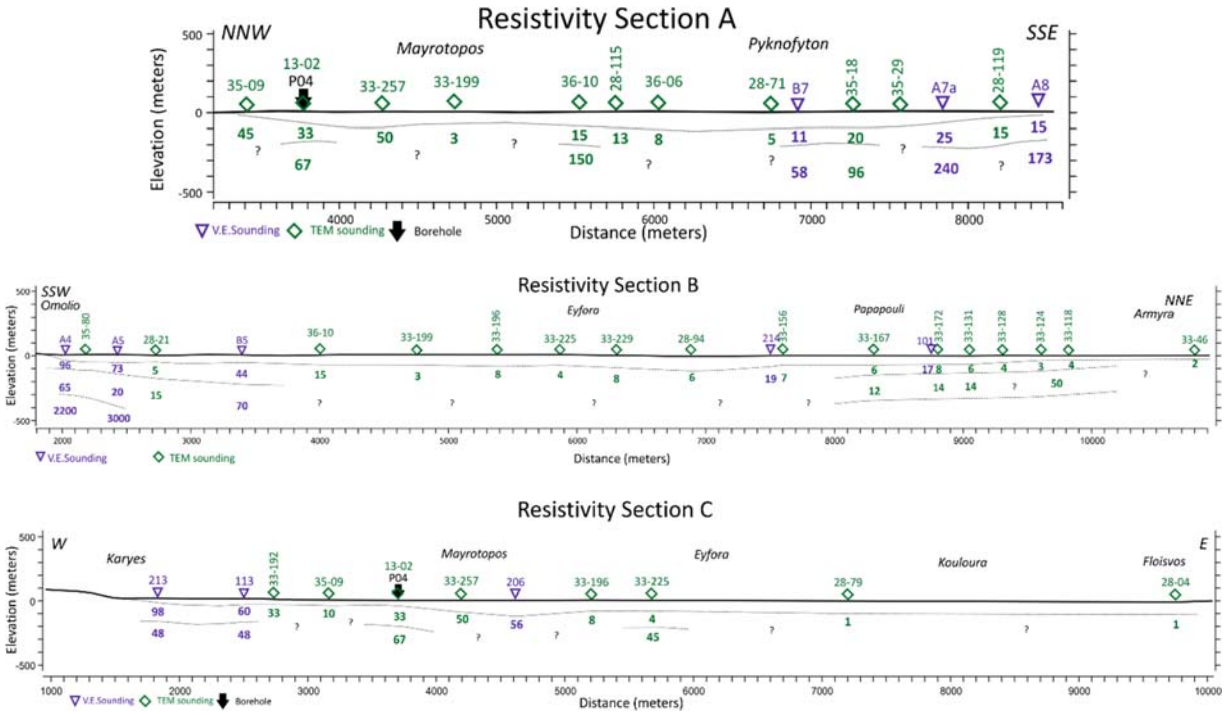

Figure 19. The three combined geoelectrical sections with the 1-D calculated geoelectrical models from both the VES and TEM soundings.

A dense grid of 127 TEM soundings (Fig.1) was carried out covering the entire deltaic plain (Alexopoulos *et al*., 2019a). The TEM soundings were performed with ABEM's WalkTEM Time Domain Ground EM system. The field configuration for data acquisition was comprised of a 40m x 40m square transmitter loop with two in-loop antennas, the RC-200 (10m x 10m) and the RC-5 (0.5m x 0.5m) each with different receiver areas. The data processing and inversion were completed with *ViewTEM* software and resulted in a multilayer resistivity model for each TEM sounding. Every single multi-layer resistivity model was converted into a few-layer geophysical model, after grouping the observed resistivity values. An example of this procedure is presented in Fig. 17, the 'Resistivity– Elevation' chart is illustrated, presenting the same TEM sounding in both ways; as a multi-layer resistivity model and as a four-layer resistivity model.

In a few locations we have carried out both VES and TEM soundings, finding out that their interpretation results were quite similar (Fig. 18). Therefore, based on all the geoelectrical models we constructed the geoelectrical sections A, B and C, presented in Figure 19. The 1-D

calculated geoelectrical models from both the VES and TEM soundings are illustrated. These are the geoelectrical data that are taken into consideration combined with the gravity data for the final interpretation (Fig. 20)

4. Geological interpretation

4.1. Density determination

Density contrasts of geological formations are very important for the processing of the gravity data and the construction of the gravity models. Several authors (Boszczuk *et al*., 2011; Damaceno *et al*., 2017; Dilalos *et al*., 2019a; García-Pérez *et al*., 2018; Langenheim, V. E., 2019) have carried out laboratory measurements in order to determine the bulk densities of the geological formations existing in their study area. Near the surface and especially above the water table the appropriate density is usually the dry bulk one, while the saturated bulk one is more appropriate for larger depths.

For reliable determination of the densities, it is necessary to measure numerous geological specimens of each geological formation, collected from several locations in order to calculate their average value that will provide a representative value of the formation. It is preferred that the samples are taken from borehole cores since they are more characteristic than the weathered samples from surface outcrops. A set of 3 measurements is required to measure the density of hand samples or cores, that will allow us to determine the dry bulk density ρ_d, the saturated bulk density ρ_s and the granular one ρ_g.

In the framework of this research, laboratory density measurements were carried out on 302 geological specimens, collected from several locations of almost every solid formation existing in the area (Fig. 1). The precision scale used had a readability of 0.001gr.

Geological formation	**Number of specimens**	**Saturated Density (gr/cm^3)**	**Standard deviation**	**Resistivity (Ohm.m)**
Quaternary Loose deposits (Q)	-	1.90	-	5-12
Neogene formation (Ng)	21	2.20	±0.05	3-98
Blue Schists (*sch*)	60	2.85	±0.07	14-240
Crystalline Limestones (*J-K-Em.k*)	35	2.70	±0.01	150-3000
Metamorphic basic ophiolithic rocks (*ab.sch*)	131	2.75	±0.03	15-25
Serpentinites (σ)	55	2.65	±0.02	>1000

Table 1. Density and resistivity values (both VES and TEM) of each geological formation of the area.

For the Neogene deposits (Ng) that are comprised of alternations of sands, marls and conglomerates the determination of their density is impossible. Due to that reason, the assigned density value was based on the results of an almost identical formation in Athens basin that the authors have investigated thoroughly with several methods of density determination (Dilalos, 2018; Dilalos *et al*., 2019a). The simplified formation of Quaternary Loose deposits used for the geological-geophysical models is practically comprised of the alluvial deposits, the underlying clay layer and the transgressive deposits that have been deposited due to the active deltaic

conditions. Therefore, we assigned a slightly increased literature value of 1.9 gr/cm^3 (Jacoby & Smilde, 2009; Manger, 1963), based on the lithology. The errors of the adopted values for each formation/lithology are also illustrated in Table 1. The density values illustrated in this table will be assigned to each block/prism in the next section, in order to construct the Interpretative 2.75D models.

4.2. Interpretative models

Interpretative geological-geophysical profiles have been constructed, with the contribution of **GM-SYS** by *Geosoft* (Dilalos *et al*., 2019a; 2019b; Dilalos & Alexopoulos, 2019b; 2020; Langenheim, V. E., 2019; Weidmann *et al.,* 2016). The gravity response from a geological cross-section is calculated and compared to the observed field anomaly response.

In Figure 21, the location of the profiles along the deltaic area, selected to create the interpretative models, is presented. Three (3) sections have been constructed (Fig. 20) in order to contribute to the adumbration of the tectonic framework of the area. In each of these figures, the upper part illustrates the observed residual gravity data (squares) along with the calculated one (line) based on the geological model, which is illustrated on the lower part of the figures. The sections are presented with a scale 1:2; therefore, there is a vertical exaggeration for better presentation and understanding. The first number in the brackets of each block/geological formation indicates its density while the second one (where applicable) indicated its corresponding resistivity.

These interpretative profiles have been constructed by taking into consideration all the information derived from the processing of all the applied geophysical methods in the area and of course the geology of the area. We began constructing these interpretative geological profiles with an initial geological model based on the literature and authors' personal geological data. Importing the calculated and assigned density values of each geological formation (§4.1), as a geological constrain, allowed the calculation of the gravity response of each section's geological model. Afterwards, we carried out iterative efforts of improving the models, whenever it was possible, taking always into consideration the geology of the area. The scope was to improve the fit of the gravity response of the model with the observed one. Beyond these, the geologically interpreted results of the VES and TEM soundings were also taken into account, improving and constraining the interpretative geological models for the shallower depths. Finally, we also had as a constrain the geological information of the borehole P04.

The integrated interpretation had as an initial input the results of the gravity data processing, given the fact that this method can provide information for greater depths (up to 3,370 meters based on 3D inversion). The geoelectrical and geoelectromagnetic methods seem to reach relatively smaller depths of investigation (up to 250-300 meters). The geological interpretation of the VES and TEM data is practically based on the layered model of each station (Alexopoulos, 2014; Alexopoulos *et al*., 2014a; 2014b; 2019) along with some re-evaluations based on the gravity results. These data were taken into account in order to calibrate or/and control the gravity interpretation (García-Pérez *et al*., 2018).

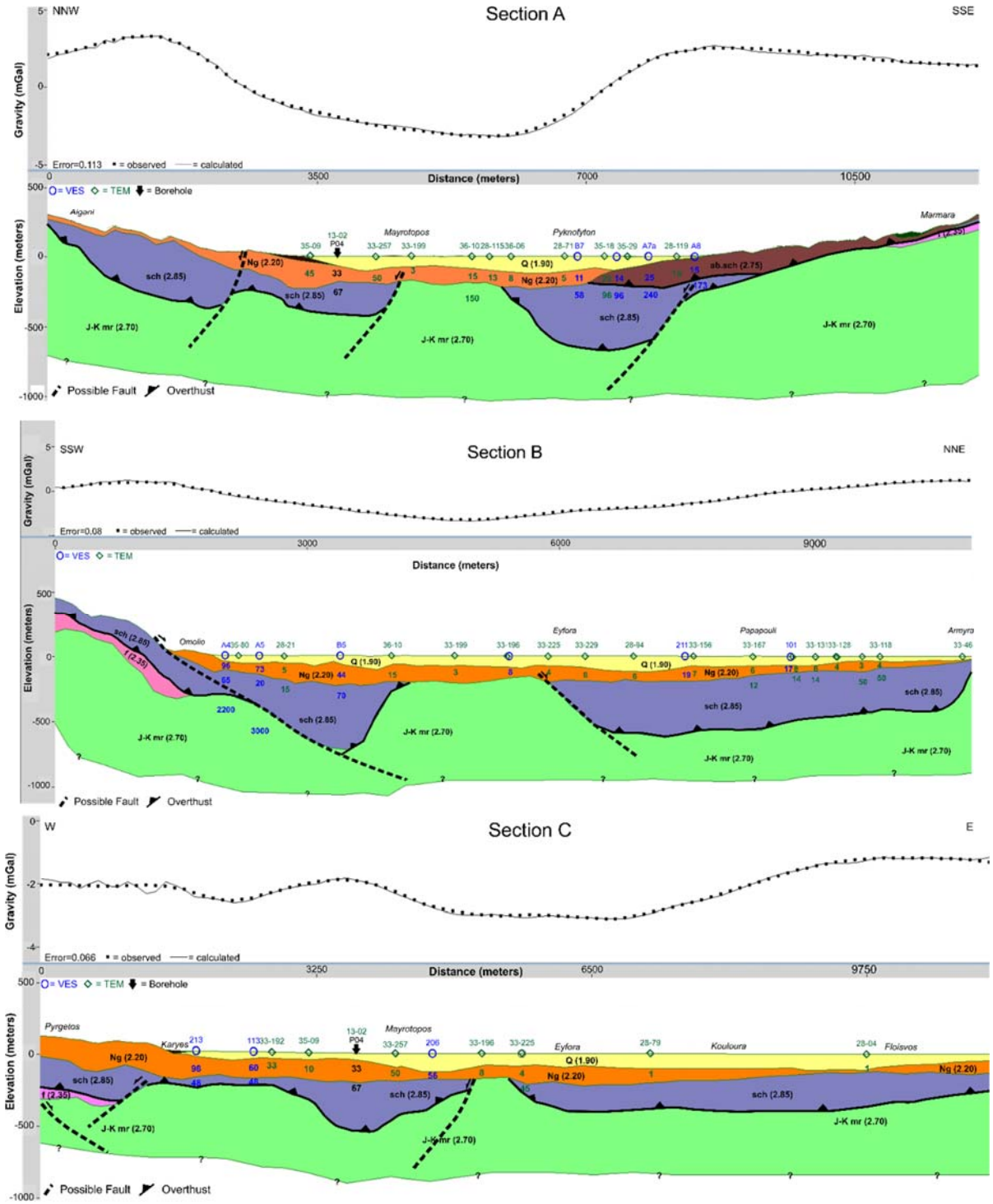

Figure 20. Interpretative geological 2.75-D profiles (*scale 1:2*). The observed (*squares*) and calculated (*line*) residual anomaly are illustrated. The number in the brackets indicates the selected density of each geological formation. The VES are illustrated with blue circles, while the TEM with green rhombus. Below them, we can observe their resistivities in blue and green font correspondingly. Finally, the black arrow illustrates the boreholes. The geological formations are: **Q**: Quaternary loose deposits, **Ng**: Neogene deposits, **J-K-Em.k**: Crystalline limestones, **sch**: Blue schists, **ab.sch**: Amphibolites, **f:** flysch.

The VES and TEM soundings have adumbrated the geological contact representing the bottom of the Quaternary Loose deposits and roof of the Neogene deposits across all the profiles. Beyond that, we have data that allow us to delineate the next geological contact representing the bottom of the Neogene deposits and the roof of the alpine basement, which is either the Blue schist (sch) or the Crystalline limestones (J-K-Em.k). This geological contact was investigated by VES and TEM soundings, mainly along section A and in smaller extent along sections B and C, probably due to the smaller investigation depths of their involved soundings. We can observe that from the TEM soundings the resistivity values are quite lower regarding the VES ones, even at the same area. which is quite common and has been faced by several authors (Meju, 2005; Meju et al., 1999). We could say that in our case the resistivity values from TEM soundings is almost half of the VES ones. In all three Sections of Figure 20, the Neogene deposits (*Ng*) are observed with thickness, up to 230 meters covering almost all the deltaic valley. Overlying them, we observe a layer of 120-140 meters of Quaternary Loose deposits (*Q*). A great part of the deltaic subsurface, beneath the Neogene deposits, is covered by the Blue Schists (*sch*) investigated with a maximum thickness of 645 meters. Across all these sections (Fig. 20), we can observe several concealed fault zones that seem to control the thickness and location of the Blue Schists (*sch*) formation and the Crystalline limestones (*J-K-Em.k*). These fault zones have probably controlled the geological evolution of the deltaic area and the relief of the bedrock over which the post-alpine sediments were deposited. The Crystalline limestones (*J-K-Em.k*) are either underlying directly below the Neogene deposits (*Ng*), as observed mainly in the central area of the basin or below the Blue Schists (*sch*). The first case is the one that produces the low values in the residual gravity field (down to -3.3 mGal) along with the overlying layer of Neogene deposits. In Sections B and C, we can also notice the existence of a small layer of flysch (*f*), between the Blue Schists (*sch*) and the Crystalline limestones (*J-K-Em.k*). On the other hand, the Amphibolites (*ab.sch*) are mainly observed at Section A, at the foothills of Ossa Mountain with a maximum thickness of 200 meters.

The resistivity values along the sections of Figure 20 along with previous publications of the authors (Alexopoulos, 2014; Alexopoulos *et al*., 2014a; 2014b; 2019; Matiatos *et al*., 2018), dealing with the preliminary results of the geoelectrical and geoelectromagnetic methods, indicate that the Neogene formations (*Ng*) are saturated with water. It is also important to notice that moving towards the northern and eastern part of the deltaic area the resistivity values decrease at such a level that indicate seawater intrusion (also mentioned in Alexopoulos *et al*., 2019).

5 Results and discussion

The interpretation of the collected geophysical data proved to be valuable as we have obtained new important information about the tectonic regime of the deltaic basin of Pineios river in Thessaly. The Euler deconvolution depth solutions (Figs. 4-5), for both selected Structural Indexes (0 and 1) seem to have great similarities to the structural maps. The calculated depths (159.8 and 1,716.6 meters) are ranging close to the source depths that have been estimated by the Energy Spectrum Analysis. The qualitative structural maps seem to contribute a lot to the

identification of the fault zones, helping to identify and propose new locations of blind faults (Fig. 21). This is practically accomplished by identifying through the structural maps large or small edges with large or small density contrasts (Fairhead, 2015). These density contrasts can be produced by different geological formations (with different density values). Therefore, if we have different geological formations bilaterally of these edges in the structural maps, we could interpret them as fault zones.

Beyond these, from the 3D models (Figs 14-16), we can interpret the subsurface structure of the delta for depths up to 3,370 meters. We managed to interpret all the geophysical results by constructing the geological-geophysical models (Fig. 20), based not only on the gravity response of the collected data but also on the geologically interpreted layered models of the VES and TEM soundings. The determination of the densities of the local geological formations from laboratory measurements was also important for the constrain of the geological-geophysical models.

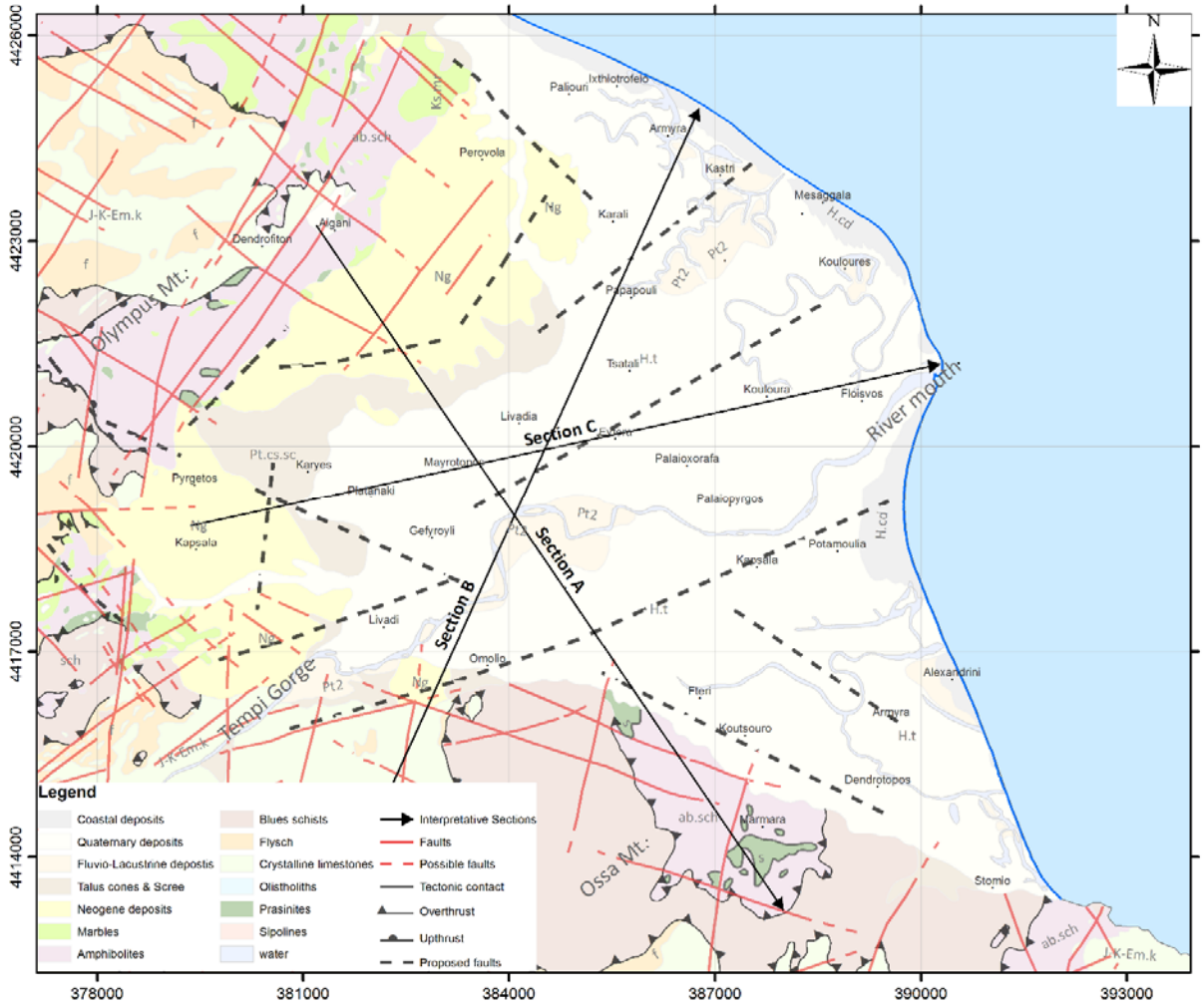

Figure 21. Updated geological and tectonic map, based on the results of the gravity survey. The locations of the new proposed fault zones are illustrated with black dashed lines and the ones of the

interpretative sections (§4.2) with solid black lines.

Therefore, based on the above results we can propose and delineate concealed possible fault zones (Fig. 21), covered by the deltaic sediments. In general, these zones are observed with two main perpendicular directions, SW-NE and NW-SE. A major tectonic zone has been adumbrated, beginning from the inner deltaic area and the end of *Tempi* gorge, passing through *Omolio* and *Potamoulia* in a SW-NE direction and ending up to the coast south of the River mouth. There are also two smaller but parallel, concealed zones to the northern area, across the areas *Gefyrouli-Eyfora-Kouloura* and *Papapouli-Kastri* and one at the inner deltaic area, close to *Livadi*.

Moreover, there is a main fault zone along the foothills of *Ossa Mt.,* with NW-SE direction, running through *Fteri, Koutsouro* and *Dendrotopos*, which may extend to the inner northwesternmost deltaic area, towards the area of *Pyrgetos*. Additionally, a smaller fault zone has been revealed northeastermost, close to *Almyra*. Finally, a set of smaller concealed fault zones, with altering directions, have been adumbrated across the foothills of *Olympus Mt.* and the hilly area of the Neogene deposits.

In terms of the tectonic evolution of the contemporary Pineios deltaic area we argue that from Pliocene to Early Pleistocene, long before the Tempi gorge was formed and used as a water pathway by Pineios river to reach the ocean. The area was below the sea level and under extension along the NE-SW direction, possibly related to the post-orogenetic phase of the orogenic collapse (Caputo, 1990; Caputo *et al*., 1994). During this phase the NW-SE striking normal faults are being active causing the gradual uplift of Ossa Mt. The main structure is the marginal fault that bounds the present deltaic plain and its trace is passing through Pyrgetos and the foothills of Ossa Mt. (*Fteri, Koutsouro and Dendrotopos*). Based on the geophysical results, a series of smaller faults, which were revealed within the river delta and are striking more or less in the same direction. These are also active during this extensional event, as they belong to the same stress field and will be covered by river deposits in a later phase. At the same time the tilting of Neogene marine formations takes place, resulting in the inclination of blocks about 10^{o} towards SSE. On top of these blocks the reddish Late Pleistocene formations, which are cropping out near Pyrgetos are being deposited unconformably. We argue that the origin of this material is continental and is transported by the river creating a small alluvial fan at the westernmost part of the study area, during that period.

A post-Pleistocene change at the direction of tectonic extension marks the following phase that affects the area. The new stress field with NW-SE direction of extension is the main cause for the generation of NE striking normal faults. The main structure passes through the location that *Omolio* village is established today and was described earlier in this manuscript. There are also smaller structures parallel to this one, which were also revealed through this research and belong to the same stress field. The implications of this stress field were either the segmentation of the *Pyrgetos* fault (described above) and the further block tilting (including the unconformity mentioned before) for another 10^{o} towards S. The latter caused the Neogene's bedding to be found today inclined at the values of 20^{o}-30^{o}. In general, above the alpine basement rocks the

inclined Neogene deposits (*Ng*) are generally observed (Fig. 20) and within the deltaic basin, the alluvial deposits, controlled mostly by the river flow, are overlying.

During this later phase, the most significant event happened as the combination of several tectonic structures allowed the Tempi gorge to widen, connecting the palaeo-lake of Larissa (Faugères, 1977; Caputo *et al*., 1994), which was filled with water up to Late Pleistocene with the Aegean sea and shortly after the contemporary Pineios river delta began to form and expand till today. The present deltaic area is gradually filling up with river deposits and consequently most of the faults are being covered and are possibly inactive as the contemporary stress field is altered (Caputo *et al*. 2012).

The maximum subsurface thickness of the investigated geological formations existing across the deltaic area, derived from the interpretative sections (Fig. 20), are provided below:

- Quaternary Loose deposits (*Q*): up to 120-140 meters.
- Neogene formations (*Ng*): up to 230 meters,
- Blue Schists formation (*sch*): up to 645 meters.
- Amphibolites (*ab.sch*): up to 200 meters.

As we have already mentioned, only one geophysical study was carried out in the area (Atzemoglou, 2010) before the one presented in this paper, regarding a set of Vertical Electrical Soundings. Its scope was only the hydrogeological study of the area and was restricted to the foothills of Ossa Mt. On the other hand, some previous geological studies had been focused on the surface geological and geomorphological mapping, without investigating the subsurface. Taking these facts into consideration, the authors believe that the significance of the present study is quite important, since we managed to investigate the deeper subsurface geological and tectonic structure of the deltaic valley of Pineios river. The geophysical results allowed us to propose and delineate concealed possible fault zones (Fig. 21), covered by the deltaic sediments. The results from the interpretation of the geophysical data, allowed us to geologically interpret the subsurface structure of the valley for depths of several hundred meters, valuable for the reconstruction of the palaeo-relief on top of which the modern delta has been formed. This could not be achieved with the previous geological and geophysical data of the area.

6 Conclusions

Taking into consideration that deltas are usually areas of intense geological processes, the causes of which are not always obvious, we argue that these new proposed fault zones that have been revealed from the geophysical survey, have controlled the geological evolution of the deltaic area as well as the concealed basement relief.

There have been several applications of geophysical methods (as presented earlier) across deltaic environments but mostly concerning hydrogeological purposes. Such a combination of geophysical methods has not been applied for structural purposes in deltaic valleys. The combination of gravity, geoelectrical and geoelectromagnetic data, with the structural mapping

and their jointed interpretation seems to be an ideal methodology for solving such complex geological problems. The new information revealed from this procedure can provide the keys for understanding the environmental pressure parameters.

In the case study described in this manuscript, the combined geophysical survey and especially the interpretative sections (Fig. 20), not only provided new information for the tectonic structure but also for the hydrogeological conditions of the geological formations. More specifically, it seems that the Neogene formations (*Ng*) are saturated with water, fresh is the inner area of the delta valley and probably more brackish at the outer area, probably due to seawater intrusion.

7 Acknowledgments

Part of this work (VES soundings) was financially supported by the project DAPHNE (MIS: 375908), which was co-funded by Greece and the European Union through the O.P. "*Education and lifelong learning, 2007-2013*" of the Ministry of Education and Religious Affairs. Another part of this work (TEM soundings) was financially supported by the project AGROCLIMA (11SYN_3_1913) that is funded by the Action "Cooperation 2011-2015" of the Operational Program "*Competitiveness and Entrepreneurship*" co-funded by the European Regional Development Fund (ERDF) and the General Secretariat for Research and Technology (Hellenic Ministry of Education). The authors would also like to thank Ms. Mitsika G., Ms. Kalaboki E., Dr Farangitakis P., Mr. Bazionis G., Mr. Andreadis O., Ms. Kaplanidi H. and Dr. Mavroulis S. for their valuable contribution to the field survey.

8 References

Alexopoulos, J., 2014. The contribution of the geo-electrical parameters distribution in the investigation of the paleo geographical evolution of the deltaic plain of Pineios river (Thessaly). In: *Proceeding of 10th Congress of the Hellenic Geographical Society*, 1717-1723, Thessaloniki, Greece.

Alexopoulos, J, Dilalos, S, Vassilakis, E, Michelioudakis, D, Mavroulis, S, Poulos, S., 2014a. Preliminary evaluation of geophysical and geological data in Pinios River Delta plain (Thessaly). In: *Proceeding of 10th Congress of the Hellenic Geographical Society*, 1724-1731, Thessaloniki, Greece.

Alexopoulos, JD, Matiatos, I, Dilalos, S, E. V, Panagopoulos, A, Ghionis, G, Poulos S., 2014b. Investigation of the phreatic aquifer development at the Pinios Delta basin (Thessaly), through a combination of geophysical and hydrogeological data. In: *Proceeding of 10th Congress of the Hellenic Geographical Society*, 1130-1139, Thessaloniki, Greece.

Alexopoulos, J.D., Dilalos, S., Mitsika, G.S., 2017. Preliminary results of the application of Transient Electromagnetic Method in the area of Karla lake (East Thessaly basin, Greece). *Proceedings of 11th International Hydrogeological Congress*, 2, 103-112, Athens, Greece.

Alexopoulos, J.D., Dilalos, S., Mitsika, G.S., Poulos SE., 2019a. Mapping of deltaic aquifers with the combined application of DC and TEM soundings. In: *Near Surface Geoscience 2019-25th European Meeting of Environmental and Engineering Geophysics*, We_25_P13, 5p. https://doi.org/10.3997/2214-4609.201902468

526 Alexopoulos, J.D., Dilalos, S., Mitsika, G.S., Vassilakis, Em., Poulos, S.E., 2019b. A
527 geophysical approach to the phenomenon of ground fissures at the East Thessaly basin (Greece).
528 In: *Near Surface Geoscience 2019-25th European Meeting of Environmental and Engineering*
529 *Geophysics*, 5p, https://doi.org/10.3997/2214-4609.201902379
530 Ali, M.Y., Fairhead, J.D., Green, C.M., Noufal, A., 2017. Basement structure of the United Arab
531 Emirates derived from an analysis of regional gravity and aeromagnetic database.
532 *Tectonophysics*, 712-713, 503-522. https://doi.org/10.1016/j.tecto.2017.06.006
533 Andersson, M. & Malehmir, A., 2018. Internal architecture of the Alnö alkaline and carbonatite
534 complex (central Sweden) revealed using 3D models of gravity and magnetic data.
535 *Tectonophysics*, 740-741, 53-71. https://doi.org/10.1016/j.tecto.2018.05.008
536 Anudu, G.K., Stephenson, R.A., Macdonald, D.I., Oakey, G.N., 2016. Geological features of the
537 northeastern Canadian Arctic margin revealed from analysis of potential field data.
538 *Tectonophysics*, 691, 48-64. https://doi.org/10.1016/j.tecto.2016.03.025
539 Atzemoglou A., 2010. Geophysical research at the aquifer systems 0805-0806-0807-0812.
540 *Institute of Geological and Mineral Exploration*. 162p., Thessaloniki, Greece.
541 Azizi, M. & Saibi, H., 2015. Integrating gravity data with remotely sensed data for structural
542 investigation of the Aynak-Logar Valley, eastern Afghanistan, and the surrounding area. IEEE
543 *Journal of Selected Topics in Applied Earth Observations and Remote Sensing*, 8(2), 816-824.
544 Doi: 10.1109/JSTARS.2014.2347375
545 Barsukov, P. O. & Fainberg, E. B., 2020. Mapping bedrock topography and moraine deposits by
546 transient electromagnetic sounding: Oslo graben, Norway. *Near Surface Geophysics*, 18(2), 123-
547 133. https://doi.org/10.1002/nsg.12070
548 Behera, L., Sain, K., Reddy, P. R., 2004. Evidence of underplating from seismic and gravity
549 studies in the Mahanadi delta of eastern India and its tectonic significance. *Journal of*
550 *Geophysical Research: Solid Earth*, 109(B12), B12311. https://doi.org/10.1029/2003JB002764
551 Bersi, M., Saibi, H., Chabou, M.C., 2016. Aerogravity and remote sensing observations of an
552 iron deposit in Gara Djebilet, southwestern Algeria. *Journal of African Earth Sciences*, 116, 134-
553 150. https://doi.org/10.1016/j.jafrearsci.2016.01.004
554 Boszczuk, P., Cheng, L.Z., Hammouche, H., Roy, P., Lacroix, S., Cheilletz, A., 2011. A 3D
555 gravity data interpretation of the Matagami mining camp, Abitibi Subprovince, Superior
556 Province, Québec, Canada: Application to VMS deposit exploration. *Journal of Applied*
557 *Geophysics*, 75(1), 77-86. https://doi.org/10.1016/j.jappgeo.2011.06.031
558 Caputo, R., 1990. Geological and structural study of the recent and active brittle deformation of
559 the Neogene-Quaternary basins of Thessaly (Central Greece). *Scientific Annals*, Aristotle
560 University of Thessaloniki, 12, pp. 252.
561 Caputo, R., Bravard, J-P, Helly, B., 1994. The Pliocene-Quaternary tecto-sedimentary evolution
562 of the Larissa Plain (Eastern Thessaly, Greece). *Geodinamica Acta* (Paris), 1994, 7, 4, 219-231.
563 https://doi.org/10.1080/09853111.1994.11105267
564 Caputo, R., Chatzipetros, A., Pavlides, S., Sboras, S., 2012. The Greek Database of Seismogenic
565 Sources (GreDaSS): state-of-the-art for northern Greece. *Annals of Geophysics*, 55, 5, 2012;
566 https://doi.org/10.4401/ag-5168

Damaceno, J.G., de Castro, D.L., Valcácio, S.N., Souza, Z.S., 2017. Magnetic and gravity modeling of a Paleogene diabase plug in Northeast Brazil. *Journal of Applied Geophysics*, 136, 219-230. https://doi.org/10.1016/j.jappgeo.2016.11.006

Dilalos, S., 2018. Application of geophysical technique to the investigation of tectonic structures in urban and suburban environments. A case study in Athens basin. *Ph.D. Thesis*, National and Kapodistrian University of Athens, 321p. Athens, Greece.

Dilalos, S. & Alexopoulos, J.D., 2017. Indications of correlation between gravity measurements and isoseismal maps. A case study of Athens basin (Greece). *Journal of Applied Geophysics*, 140, 62-74. https://doi.org/10.1016/j.jappgeo.2017.03.012

Dilalos, S. & Alexopoulos, J.D., 2019a. Urban Gravity Measurements for the Subsurface Investigation of Athens Basin (Greece). *Bulletin of the Geological Society of Greece,* Special Publication, 7, 211-212, GSG2019-093.

Dilalos, S. & Alexopoulos, J.D., 2019b. Quantitative subsurface information of Athens basin (Greece) derived from urban gravity measurements. In: *Near Surface Geoscience 2019-1st Conference on Geophysics for Infrastructure Planning Monitoring and BIM*, We_INFRA_P23. https://doi.org/10.3997/2214-4609.201902560

Dilalos, S., & Alexopoulos, J.D., 2020. The contribution of an urban gravity survey to the determinable perspective of Athens city (Greece) underground structure. *SN Applied Sciences*, 2(11), 1-20. https://doi.org/10.1007/s42452-020-03466-8

Dilalos S. & Alexopoulos J.D., 2021. Some new insights on the correlation of isoseismal maps with terrestrial and satellite gravity data. *11th Congress of the Balkan Geophysical Society*. 1-5. https://doi.org/10.3997/2214-4609.202149BGS17

Dilalos, S., Alexopoulos, J.D., Tsatsaris, A., 2018. Calculation of Building Correction for urban gravity surveys. A case study of Athens metropolis (Greece). *Journal of Applied Geophysics*. 159(C), 540-552. https://doi.org/10.1016/j.jappgeo.2018.09.036

Dilalos, S., Alexopoulos, J.D., Lozios, S., 2019a. New insights on Athens basin (Greece) subsurface geological and tectonic structure, derived from urban gravity measurements. *Journal of Applied Geophysics*. 167(C), 73-105. https://doi.org/10.1016/j.jappgeo.2019.04.024

Dilalos, S., Alexopoulos, J.D., Lozios, S., 2019b. The contribution of urban gravity survey to the subsurface geological structure of the Athens basin (Greece). In: *Near Surface Geoscience 2019-25th European Meeting of Environmental and Engineering Geophysics*, We_25_P17. https://doi.org/10.3997/2214-4609.201902472

ElGalladi, A.A., Ghazala, H.H., Ibraheem, I.M., Ibrahim, E.H., 2009. Tectonic interpretation of gravity field data of west of Nile Delta region, Egypt. *NRIAG Journal of Geophysics*, Special Issue, 487-508.

Fairhead, J.D., & Okereke, C.S., 1987. A regional gravity study of the West African rift system in Nigeria and Cameroon and its tectonic interpretation. *Tectonophysics*, 143(1-3), 141-159. https://doi.org/10.1016/0040-1951(87)90084-9

Fairhead J.D., 2015. *Advances in Gravity and Magnetic Processing and Interpretation*. EAGE Publications, The Netherlands, 338p. ISBN 978-94-6282-175-0

Faugères, C., 1977. Naissance et développement du relief de l' Olympe (Grèce): une manifestation éclatante de la tectonique récente. *Rev. Géogr. Phys. Géol. Dyn.*, XIX, 1, p. 7-26.

Gaki-Papanastassiou, K., Cundy, A.B., Maroukian, H., 2011. Fluvial versus tectonic controls on the late Holocene geomorphic and sedimentary evolution of a small Mediterranean fan delta system. *The Journal of Geology*, 119(2), 221–234. https://doi.org/10.1086/658144

García-Pérez, T., Marquardt, C., Yáñez, G., Cembrano, J., Gomila, R., Santibañez, I., Maringue, J., 2018. Insights on the structural control of a Neogene forearc basin in Northern Chile: A geophysical approach. *Tectonophysics*. 736, 1-14. https://doi.org/10.1016/j.tecto.2018.04.003

Hospers, J., 1965. Gravity field and structure of the Niger delta, Nigeria, West Africa. *Geological Society of America Bulletin*, 76(4), 407-422. https://doi.org/10.1130/0016-7606(1965)76[407:GFASOT]2.0.CO;2

Jacoby W. & Smilde P.L., 2009. *Gravity Interpretation: Fundamentals and Application of Gravity Inversion and Geological Interpretation*. Springer-Verlag Berlin Heidelberg. 395p. ISBN: 978-3-540-85328-2.

Ibraheem, I.M., El-Qady, G.M., ElGalladi, A., 2016. Hydrogeophysical and structural investigation using VES and TDEM data: a case study at El-Nubariya–Wadi El-Natrun area, west Nile Delta, Egypt. *NRIAG Journal of Astronomy and Geophysics*, 5(1), 198-215. https://doi.org/10.1016/j.nrjag.2016.04.004

Karymbalis, E., Gaki-Papanastassiou, K., Tsanakas, K., Ferentinou, M., 2016. Geomorphology of the Pinios River delta, Central Greece. *Journal of maps*, 12(sup 1), 12-21. https://doi.org/10.1080/17445647.2016.1153356

Katsikatsos, G. & Migiros, G., 1982. Rapsani Sheet—Geological Map in Scale 1: 50,000. *Institute of Geology and Mineral Exploration*: Athens, Greece.

Khalil, M.A. & Santos, F.A.M., 2011. 2D resistivity inversion of 1D electrical-sounding measurements in deltaic complex geology: application to the delta Wadi El-Arish, Northern Sinai, Egypt. *Journal of Geophysics and Engineering*, 8(3), 422-433. https://doi.org/10.1088/1742-2132/8/3/003

Khalil, M.A., Santos, F.M., Farzamian, M., 2014. 3D gravity inversion and Euler deconvolution to delineate the hydro-tectonic regime in El-Arish area, northern Sinai Peninsula. *Journal of Applied Geophysics*, 103, 104-113. https://doi.org/10.1016/j.jappgeo.2014.01.012

Kovach, R.L., Allen, C.R., Press, F., 1962. Geophysical investigations in the Colorado delta region. *Journal of Geophysical Research*, 67(7), 2845-2871. https://doi.org/10.1029/JZ067i007p02845

Lazogiannis K., Poulos S., Giannouli D.H, Sifnioti D.E., Tsanakas K., Tsoutsia A., Dilalos S., Gkionis, E. Vassilakis, S. Petrakis, D. Tarasi, G. Terezakis., 2015. Morphological changes along deltaic coastline of pinios river (Thessaly). Geographies, 26, 51-58. (*in Greek*)

Langenheim, V.E., Ritzinger, B.T., Zahran, H., Shareef, A., Al-dahri, M., 2019. Crustal structure of the northern Harrat Rahat volcanic field (Saudi Arabia) from gravity and aeromagnetic data. *Tectonophysics*, 750, 9-21. https://doi.org/10.1016/j.tecto.2018.11.005

Manger, G.E., 1963. Porosity and bulk density of sedimentary rocks. *Geological Survey Bulletin,* 1114(E), 60p.

Martins-Ferreira, M.A.C., Campos, J.E.G., Von Huelsen, M.G., Neri, B.L., 2018. Paleorift structure constrained by gravity and stratigraphic data: The Statherian Araí rift case. *Tectonophysics*, 738-739, 64-82. https://doi.org/10.1016/j.tecto.2018.05.014

Matiatos I, Paraskevopoulou V, Lazogiannis K, Botsou F, Dassenakis M, Ghionis G, Alexopoulos JD, Poulos SE., 2018 Surface–ground water interactions and hydrogeochemical evolution in a fluvio-deltaic setting: The case study of the Pinios River delta. *Journal of Hydrology*, 236-249. https://doi.org/10.1016/j.jhydrol.2018.03.067

Meju M.A., 2005. Simple relative space–time scaling of electrical and electromagnetic depth sounding arrays: implications for electrical static shift removal and joint DC-TEM data inversion with the most-squares criterion. *Geophysical prospecting*, 53(4), 463-479. https://doi.org/10.1111/j.1365-2478.2005.00483.x

Meju M.A., Fontes S.L., Oliveira M.F.B., Lima J.P.R., Ulugergerli E.U., Carrasquilla A.A., 1999. Regional aquifer mapping using combined VES-TEM-AMT/EMAP methods in the semiarid eastern margin of Parnaiba Basin, Brazil. *Geophysics*, 64(2), 337-356. https://doi.org/10.1190/1.1444539

Migiros, G., Bathrellos, G.D., Skilodimou, H.D., Karamousalis, T., 2011. Pinios (Peneus) River (Central Greece): hydrological—geomorphological elements and changes during the quaternary. *Central European Journal of Geosciences*, 3(2), 215-228. https://doi.org/10.2478/s13533-011-0019-1

Morelli, C., Gantar, C., Honkasalon, T., McConnel, K., Tanner, J.G., Szabo, B., Uotila, U., Whalen, C.T., 1974. *The International Standardization Net 1971 (IGSN71)*. IUGG-IAG Publ. Spec. 4. Int. Union of Geod. and Geophysics.

Nasuti, A., Pascal, C., Ebbing, J., 2012. Onshore–offshore potential field analysis of the Møre–Trøndelag Fault Complex and adjacent structures of Mid Norway. *Tectonophysics*, 518, 17-28. https://doi.org/10.1016/j.tecto.2011.11.003

Orellana, E., Mooney, H.M., 1966. Master Tables for Vertical Electrical Soundings over Layered Structures. Interciencia, Madrid

Othman, A., Ibraheem, I. M., Ghazala, H., Mesbah, H., Dahlin, T., 2019. Hydrogeophysical and hydrochemical characteristics of Pliocene groundwater aquifer at the area northwest El Sadat city, West Nile Delta, Egypt. *Journal of African Earth Sciences*, 150, 1-11. https://doi.org/10.1016/j.jafrearsci.2018.10.011

Saleh, S., 2013. The role of geophysical and seismological data in evaluating the subsurface structures and tectonic trends of Nile Delta, Egypt. *Arabian Journal of Geosciences*, 6(9), 3201-3216. DOI 10.1007/s12517-012-0603-9

Selim, E.S.I., 2013. Subsurface structural trends of the offshore Nile Delta area, Egypt: evidences from gravity and magnetic data. *Environmental Earth Sciences*, 68, 1015-1032. https://doi.org/10.1007/s12665-012-1804-y

Syvitski, J.P., 2008. Deltas at risk. *Sustainability science*, 3(1), 23-32. Doi: 10.1007/s11625-008-0043-3

687 Torres-Rondon, L., Carriere, S. D., Chalikakis, K., Valles, V., 2013. An integrative geological
688 and geophysical approach to characterize a superficial deltaic aquifer in the Camargue plain,
689 France. Comptes Rendus Geoscience, 345(5-6), 241-250.
690 https://doi.org/10.1016/j.crte.2013.07.002
691 Vassilakis Em., Mavroulis S., Alexopoulos J.D., Dilalos S., 2014. The morphotectonic evolution
692 of the deltaic area of Pineios river (Thessaly). *Proceeding of 10th Congress of the Hellenic*
693 *Geographical Society*, 1724-1731, Thessaloniki, Greece (*in Greek*)
694 Vörösmarty, C.J., Meybeck, M., Fekete, B., Sharma, K., Green, P., Syvitski, J.P., 2003.
695 Anthropogenic sediment retention: major global impact from registered river impoundments.
696 *Global and Planetary Change*, 39(1-2), 169-190. https://doi.org/10.1016/S0921-8181(03)00023-
697 7
698 Weidmann, C., Gimenez, M., Klinger, F.L., Alvarez, O., 2016. Anomalous values of gravity and
699 magnetism in the western margin of Gondwana. *Tectonophysics*, 667, 1-15.
700 https://doi.org/10.1016/j.tecto.2015.11.017
701 Wijns, C., Perez, C., Kowalczyk, P. 2005. Theta map: Edge detection in magnetic data.
702 *Geophysics*, 70(4), L39-L43. https://doi.org/10.1190/1.1988184
703 Zohdy, A.A., 1989. A new method for the automatic interpretation of Schlumberger and Wenner
704 sounding curves. *Geophysics*, 54(2), 245-253. https://doi.org/10.1190/1.1442648